15 Parameters used on the gas temperature calculations

15.1 Substrate thermal properties as a function of temperature

During the wall heat flux calculations of the two gauges, the substrate thermal properties of the ceramic heads are assumed to remain constant. Miller (1981) investigates the influence of the thermal properties of the Macor substrate, as its temperature reaches higher values. He suggests a change on the ratio of the two thermal products of two similar Macor substrates that are at two different temperatures equal to *0.0006 / K*.

For the case described in Figure 12-3, the initial temperature difference between the two ceramic heads reached *89.9K*, while their difference at the end of the test is *129.9K*. According to Miller (1981) the thermal product of the hot head is *0.0539* times higher than the one from the cold head at the beginning of the test (and *0.0779* at the end if the hot head substrate temperature was assumed to be uniform and equal to the one measured by the gauge). The calibrated thermal product of Macor at ambient temperature is found equal to $2139\ J/(m^2Ks^{0.5})$. Hence, the gas temperature calculations are repeated by imposing the thermal product of the hot head equal to *2254* and $2306\ J/(m^2Ks^{0.5})$ (Figure 15-1). The difference between these two cases and the case of constant thermal product with temperature $2139\ J/(m^2Ks^{0.5})$ seems to be no more than *2K* on the gas temperature calculations. Although in reality, the thermal product is a function of temperature and thus changes across the radius of the head during a test, because this temperature difference of the thermal product was not studied, the thermal product was kept constant with radius for all the three above cases. Also, note that the case of Figure 12-3 contains the maximum difference of the two initial wall temperatures of the gauges that is observed for the tests in CT2 and in CT3. Thus, the influence of the thermal product as a function of temperature on the time-averaged gas temperature calculations can be considered a weak parameter for the test conditions of VKI facilities.

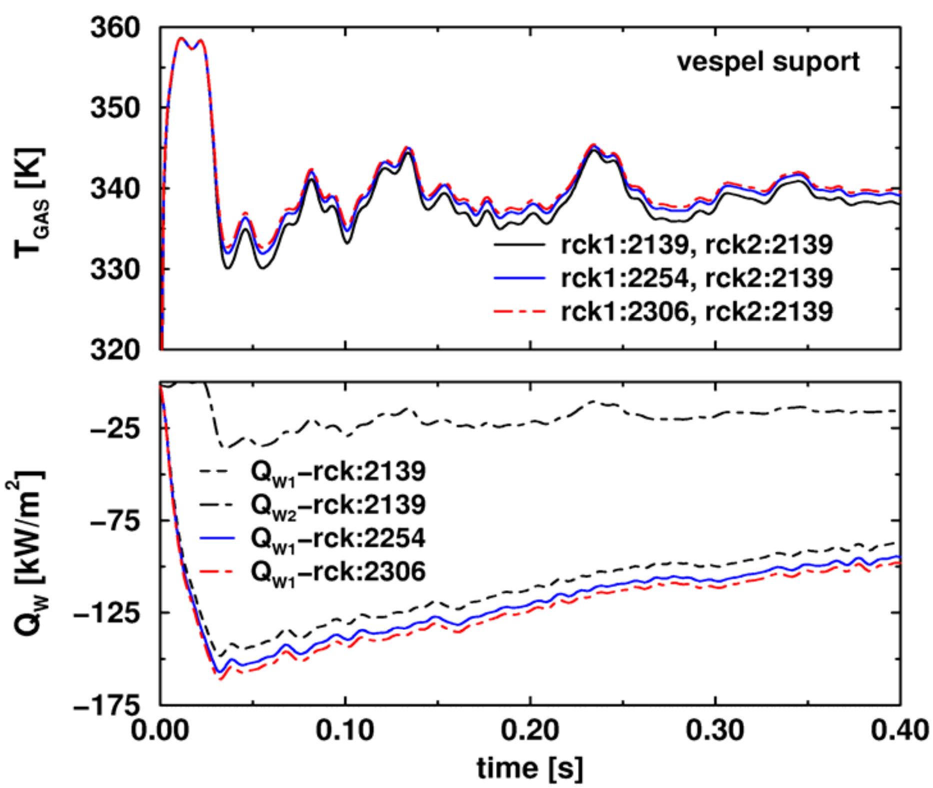

Figure 15-1: Influence of the Macor thermal product as a function of temperature on the time-averaged gas temperature calculations (test with Vespel support D.T.F.P. in CT2)

As far as the gas temperature fluctuations are concerned, it seems that they are much less influenced by the change of the thermal product value between the above limits. In Figure 15-2, the fluctuations behind the rotor are calculated for three combinations of thermal product ratios, the same as for Figure 15-1 (for comparison reasons). Thus, the error that is introduced on the gas temperature fluctuations is negligible for thermal product differences of *5-8%*.

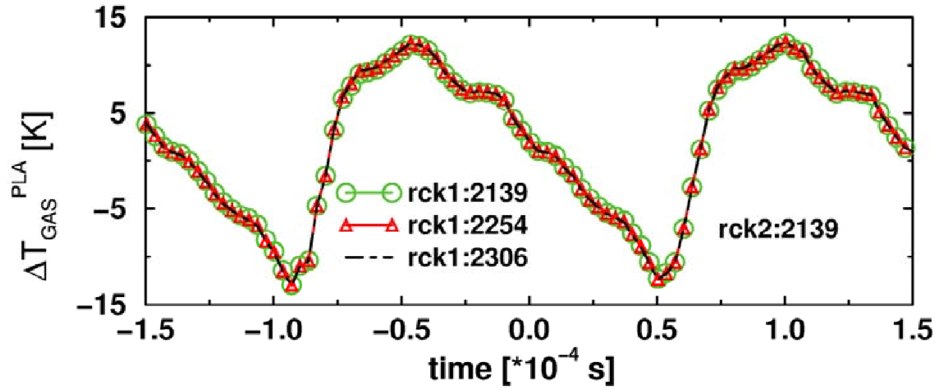

Figure 15-2: Influence of the Macor thermal product as a function of temperature on the gas temperature fluctuations (test with Vespel support D.T.F.P. in CT3 behind the rotor)

15.2 Geometry of the hemispherical heads

15.2.1 Advantages of the chosen geometry

The geometry of the heads was chosen hemi-spherical and not flat in order to avoid higher interactions between the probe and the flow, especially for higher velocities. Although cylindrical substrates in stead of hemi-spherical heads do not introduce higher interactions with the flow, the two cylindrical stagnation lines can not be on the same plane with the blade trailing edge.

15.2.2 Influence of the radius on the wall heat flux calculations

Prior to the deposit of the thin film sensor on the hemispherical heads, both heads are polished in order to avoid any high discontinuity on their surface. As a result of the polishing, the diameter of the ceramic heads is changed, especially around the stagnation area. The final two dimensional geometry of the heads of the Plexiglas support probe is measured with *1/100 mm* accuracy and shown on the top graph of Figure 15-3. (The blue line corresponds to the cold head and the red one to the hot head.) The part of the heads closer to the stagnation area (and shown in green) is approximated with a fourth order polynomial for each head and the radius of curvature (shown at the bottom graph of Figure 15-3) is calculated as the inverse of the curvature:

$$R = \frac{-\left(1 + y'^2\right)^{3/2}}{y''} \quad . \tag{57}$$

The calculated radius reached even *5 mm* for the cold head at the stagnation point. However, all the wall heat fluxes of the previous analysis are calculated based on the machined radius of *1.5mm*, prior to polishing. Thus, the influence of the chosen radius on the wall calculations and as a consequence on the gas temperature is studied: for two measurements with the Vespel support probe, the calculations are performed for three different radii of *1.5*, *5*, and *15mm*, identical for both heads (Figure 15-4). (The measurement on the left is the one already shown on the first graph of Figure 12-4, while the measurement on the right is the one shown on the first graph of Figure 12-5.) For the graph on the left (Figure 15-4), the initial wall temperature for the cold head is close to the gas temperature, contrary to the graph on the right where the gas temperature is between the two initial wall temperatures

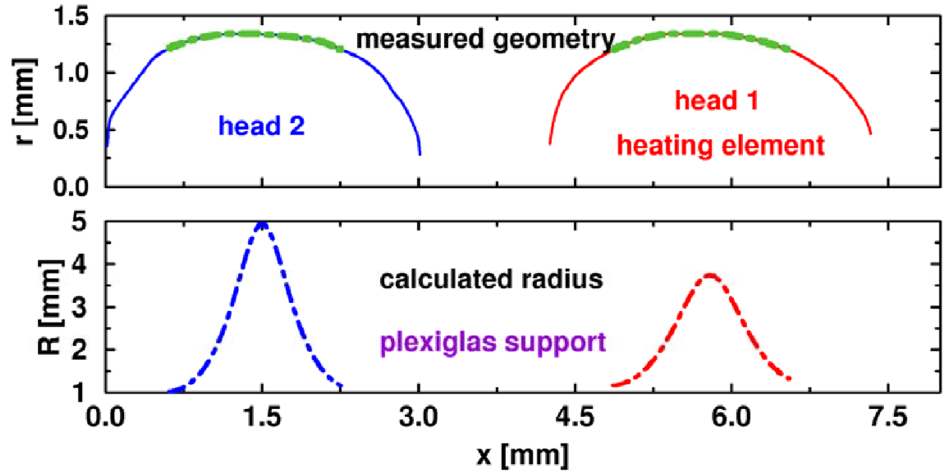

Figure 15-3: Measured geometry of the ceramic heads (top) and radius as the inverse of the curvature (bottom) (Plexiglas support D.T.F.P.)

.

The dependence of the wall heat flux on the radius seems to be somehow proportional to the absolute value of the heat flux. As a result, when both radii of the two heads experience the same increase, the gas temperature does not seem to be significantly influenced by the radii changes, as it is the wall heat flux ratio that dominates the gas temperature calculations and not the independent values of the wall heat fluxes (Eq. (45)). Thus, it is more representative to plot the wall heat flux ratios for the two measurements (Figure 15-5), and to confirm that there is no considerable difference.

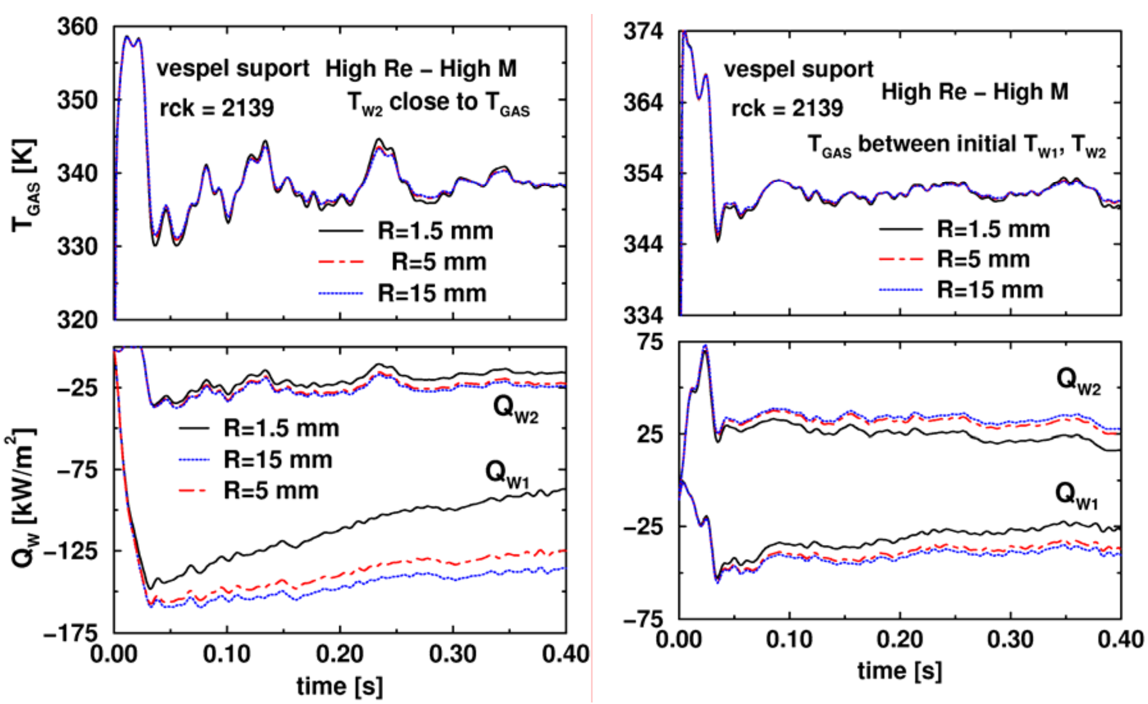

Figure 15-4: Influence of the choice of the radii whose values are the same for the two heads on the gas temperature calculations (tests with Vespel support D.T.F.P. in CT2)

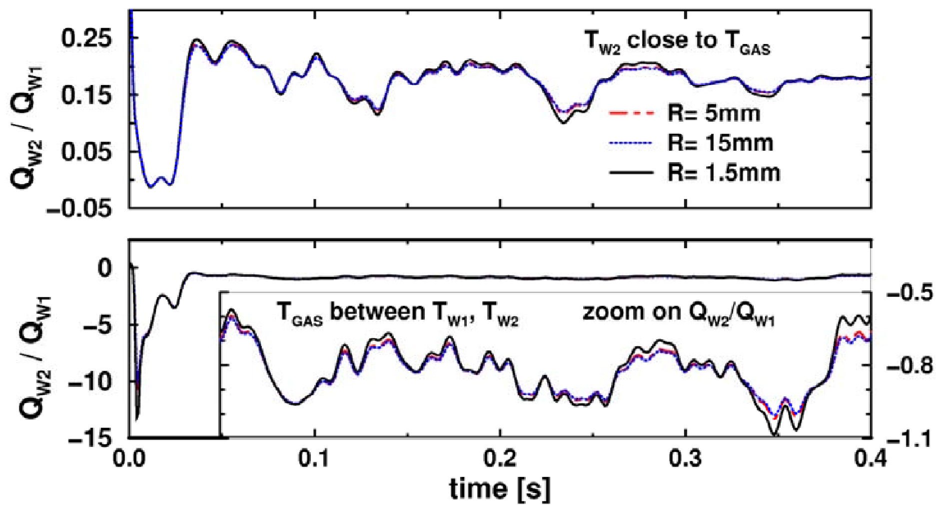

Figure 15-5: The top wall heat flux ratio corresponds to the test shown on the left of Figure 15-4 and the bottom ratio to the test on the right of Figure 15-4

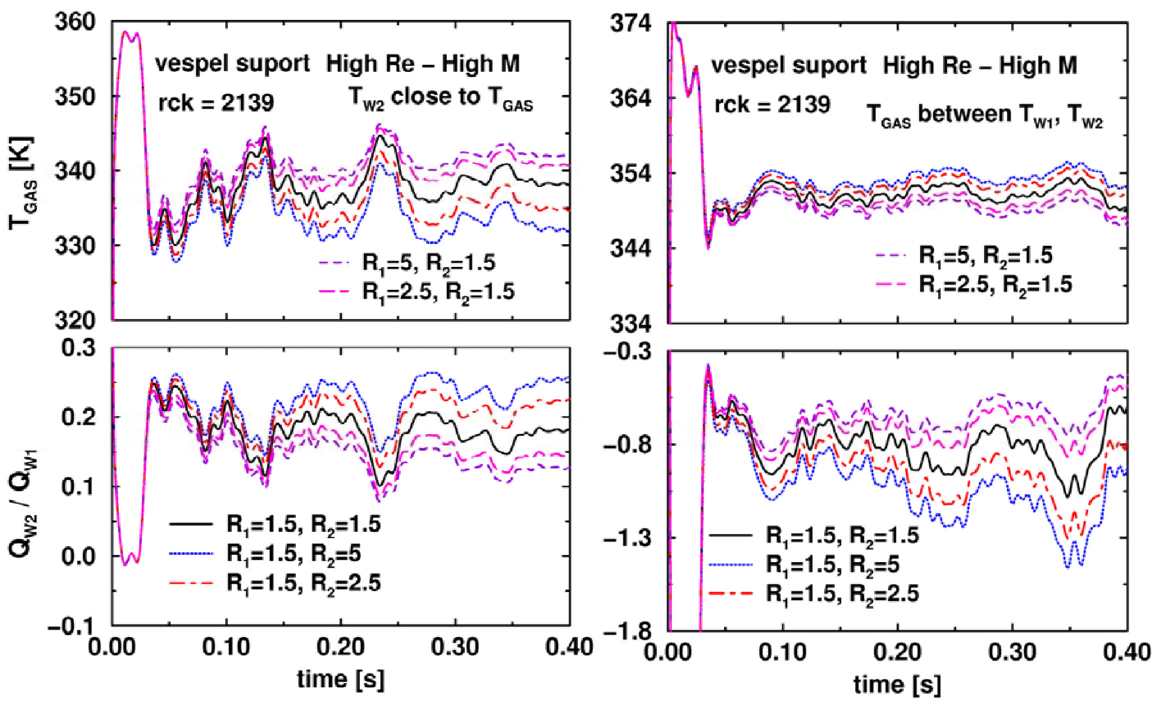

Figure 15-6: Influence of the choice of the radius of each head on the gas temperature calculations (tests with Vespel support D.T.F.P. in CT2)

The wall heat flux ratio changes significantly when the radii of the two heads are different. While keeping one of the two radii at the nominal value of *1.5mm*, the other one increases at *5mm* and *2.5mm* (Figure 15-6). Then the gas temperature is recalculated and showed on the top graphs for the two different measurements. The heat flux ratio is also plotted on the bottom graphs correspondingly. The different value of the radius does not really influence the beginning of the tests because the wall heat fluxes can be approximated with the calculations of a flat geometry (Eq. (37))). However, as the wall temperatures further diverge from their initial value, the differences get higher and higher. After *0.4s*, *2.5mm* radius for one of the heads (just *1mm* higher than the other one) introduces *2-3 K* diversity from the gas temperature calculations with the same value of radius. A second look at Figure 15-3 shows that differences of *1mm* between the two radii can be possible, mainly very close to the stagnation point, where the thin film sensor is deposited.

In general, it is very difficult to accurately determine the radius at the stagnation region of the heads (in our case, the heads geometry was approximated to a fourth order polynomial) and this is the main reason why the nominal radii of the heads are used for all the gas temperature calculations described in chapter 11, 12, 14, 13. Although the comparison of these calculations to the results from a thermocouple was satisfactory, errors on the gas temperature calculations of the order of *2K* at the end of the tests described in above paragraphs can be possible.

15.3 Two dimensional effects on the conduction inside the ceramic heads

Another source of possible error could be the existence of lateral conduction in the ceramic substrate, as the time of the experiments gets longer. The conduction equation that is used for the calculation of the heat flux through the substrate is one dimensional (1D) (Eq. (46)). As there is no two dimensional (2D) tool to compare the wall heat flux calculations between 1D and 2D, there are only the comparisons of the gas temperature measurements between the probe and the thermocouples that diminish the possibility of significant lateral conduction inside the substrates.

15.4 Heat transfer coefficient

The gas temperature calculations with the dual thin film probe are based on the first assumption that both ceramic heads feel the same flow at the same time. The heat transfer coefficient for each head is defined as the ratio of the wall heat flux over the temperature difference between the gas and the wall (Eq. (44)) and is assumed equal to both heads. As the determination of the gas temperature by the probe and the thermocouple gives very similar values, it seems that the two above assumptions do not introduce significant errors on the gas temperature calculations.

However, convection is not the only phenomenon that takes place during the test. The heating resistance inside one of the heads generates a constant heat flux that heats up both heads by conduction through the heads and their support; the wall temperatures and the corresponding wall heat fluxes depend not only on the flow but also on the conductive heat flux that is generated by the heating. Therefore, the calculation of the heat transfer coefficient from the two above quantities normally contains both heat transfer phenomena, convection and conduction, although the *h* coefficient definition is based on the pure convection law. It is impossible to separate the two heat transfer phenomena and consider only the influence of the convection, as the heating was kept on for all the tests to ensure the initial temperature uniformity in the ceramic heads, just before every test.

Thus, not only the Reynolds number but also the initial wall temperatures influence the calculated value of the heat transfer coefficient contrary to the theory of pure convection. The above dependence on the wall temperatures is illustrated in Figure 15-7. The repeatability on the gas temperature and the comparison of the heat transfer coefficient for four tests with different initial wall temperatures (different heating) performed with the Vespel support probe at high Reynolds – high Mach numbers conditions in CT2 (see Figure 12-6) is shown on the top and the bottom graph of Figure 15-7 respectively. Although the gas temperature for the fourth test is a bit lower because of the different experimental conditions from test to test, the total pressure measured upstream the cascade by a pitot probe is very repeatable (Figure 15-8). Thus, although the real convective heat transfer is the same for all the tests according to the physics, the heat transfer defined by the wall temperatures and heat fluxes of the two gauges differs. As the heating is getting stronger, the heat transfer coefficient gets lower (The ranking of the tests from the lowest to the highest heating is: 1, 4, 2, 3). This observation is better illustrated in Figure 15-9;

the average value of the heat transfer coefficient (between the test time *0.04* and *0.08s*) of the four tests is plotted as a function once of the average wall temperature of the cold head (circles) and once of the average wall temperature of the hot head (squares) (between the test time *0.05* and *0.07s*).

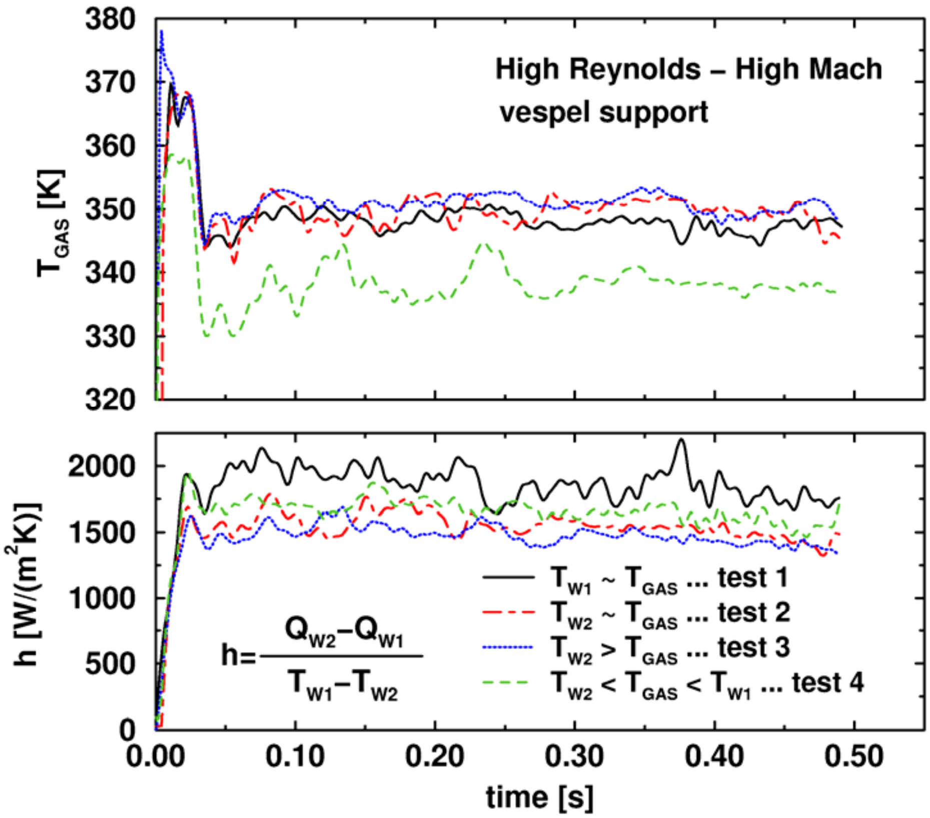

Figure 15-7: Repeatability of the gas temperature and the comparison of the heat transfer coefficient for four tests in CT2 that differ on the heating (influence of the initial wall temperatures) (Vespel support D.T.F.P.)

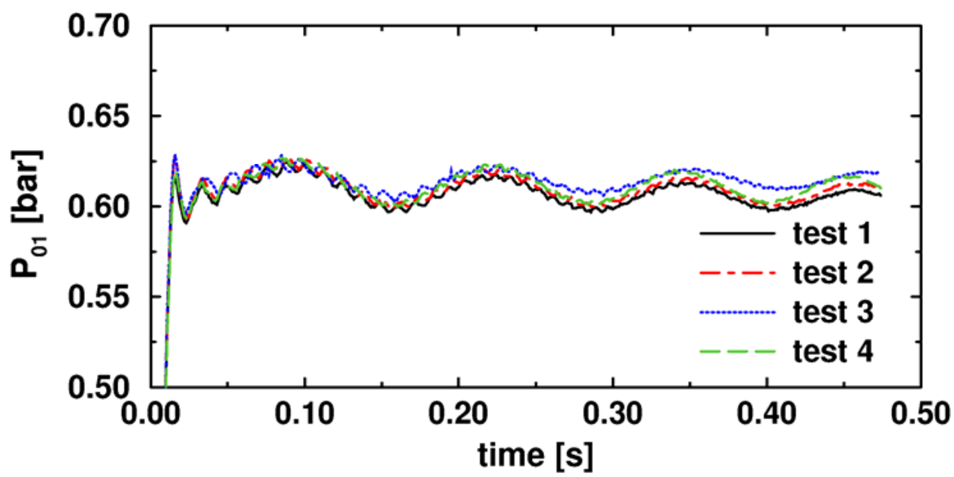

Figure 15-8: Repeatability of the total pressure upstream the cascade for the high Reynolds number conditions of the CT2 tests with the Vespel support D.T.F.P.

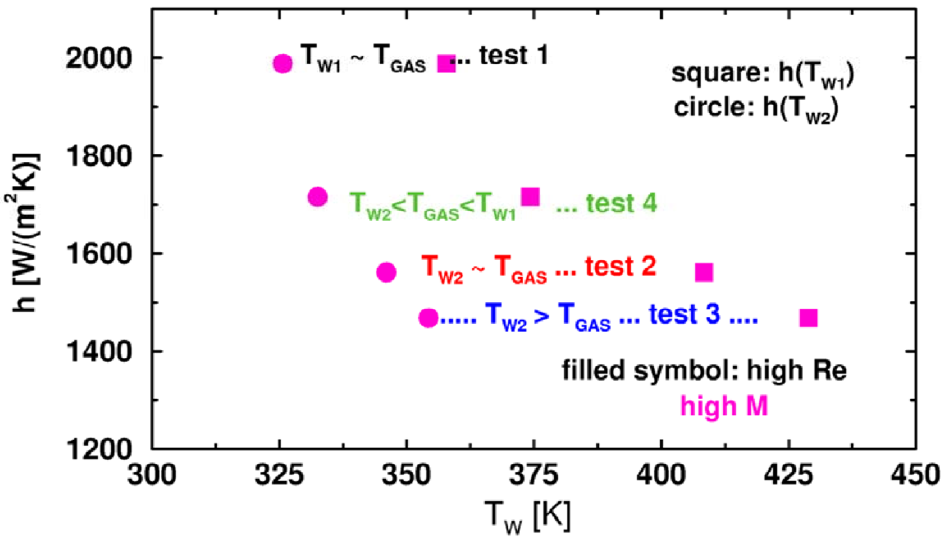

Figure 15-9: Heat transfer coefficient as a function of wall temperatures for the high Reynolds-high Mach numbers case of the CT2 tests with the Vespel support D.T.F.P.

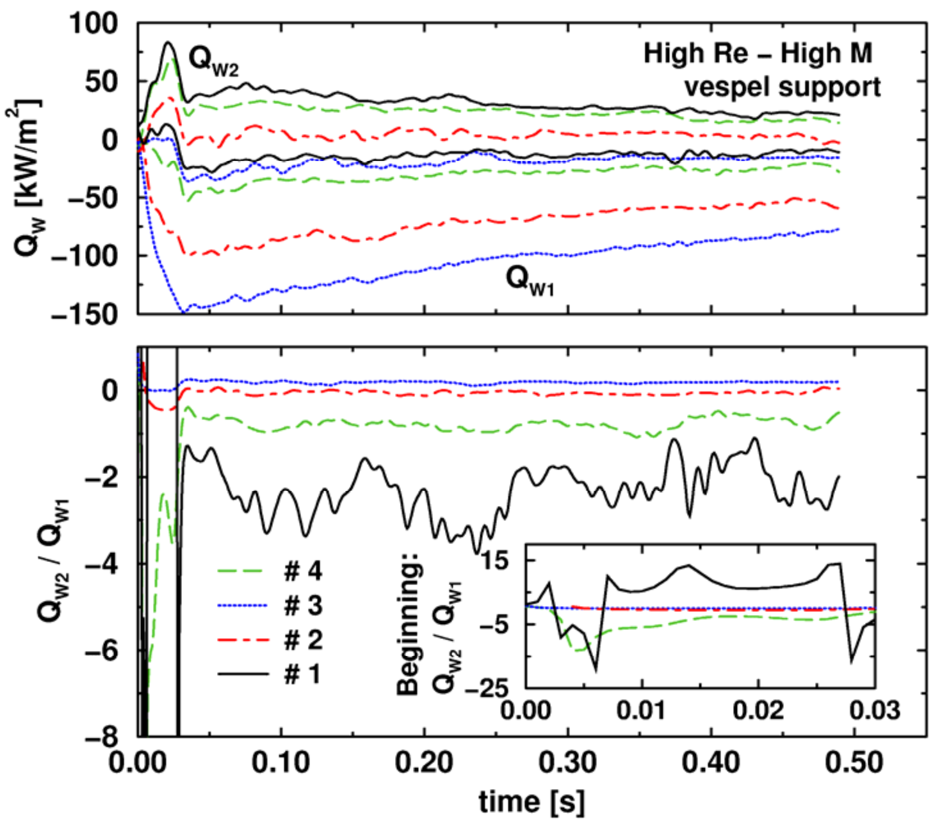

Figure 15-10: Comparison of the wall heat fluxes and their ratio for four repeatable tests in CT2 that differ on the heating (influence of the initial wall temperatures) (Vespel support D.T.F.P.)

More information is possible to be obtained from the wall heat fluxes (top graph) and their ratio (bottom graph) shown in Figure 15-10. Every different heating introduces different correlations between the two wall heat fluxes resulting in different contour on their equivalent ratios. For the CT3 tests described in chapter 14.3.1 and 14.4.1, the heating is not very different from test to test to change the contour of the wall heat fluxes and thus to influence the repeatability of the heat transfer coefficient. For the CT2 tests, the initial wall temperature conditions change drastically compared to the gas temperature. The initial wall temperature of the hot head is close to the gas temperature for test 1 (Figure 15-9). The gas temperature is between the two initial wall temperatures for test 4 and the wall temperature of the cold head reaches the gas temperature at test 2. At last, at test 3, the cold head is much hotter than the gas temperature. (Note that the beginning of the heat flux ratio is shown on the bottom-right graph of Figure 15-10 for times similar to the ones when the peak on the gas temperature in CT2 has occurred.)

Figure 15-11 is based on the same concept as Figure 15-9; the influence of the heating (through the wall temperatures) and of the test conditions (Reynolds and Mach numbers) on the average heat transfer coefficient is shown for all the tests in CT2 with the Vespel support probe. The heat transfer coefficient versus the wall temperature of the cold head is shown with the circles and versus the wall temperature of the hot head with the squares. The filled symbols represent all the tests with high Reynolds number contrary to the open symbols that stand for the low Reynolds number case. The two different colors of the symbols show the possible dependence on the Mach number.

The heat transfer coefficient always decreases as the heating increases for every operating test condition. It is also higher for the high Reynolds number (increases as the convection gets stronger) and somehow seems to be slightly dependent on the Mach number.

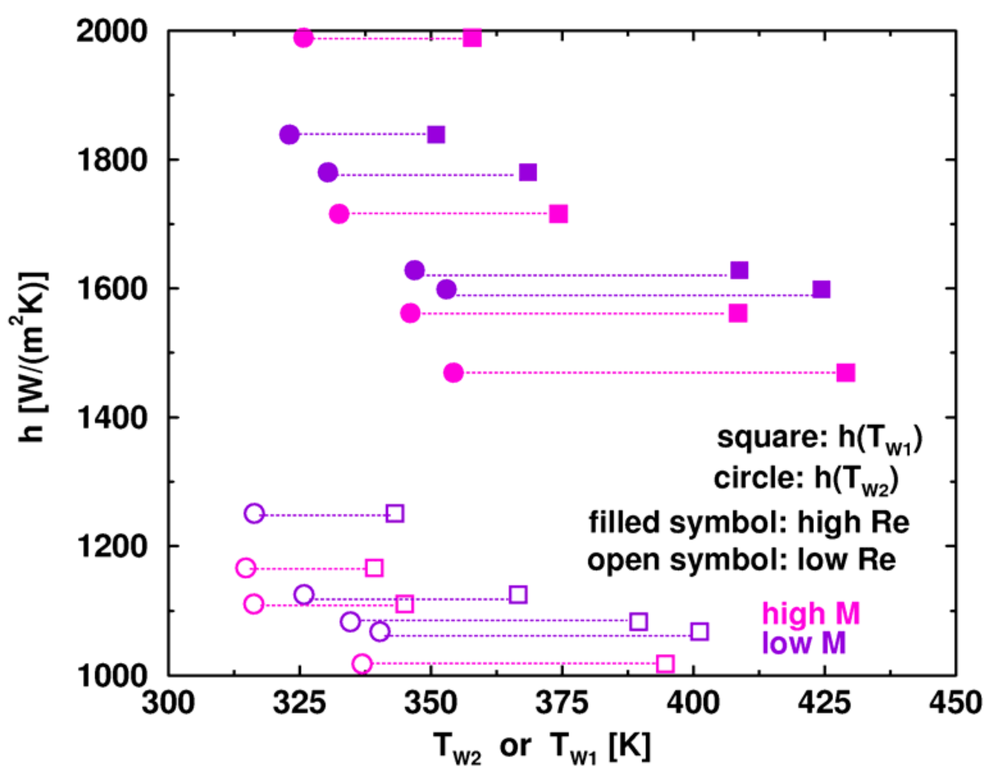

Figure 15-11: Heat transfer coefficient as a function of wall temperatures, Reynolds and Mach numbers (operating test conditions)

15.5 Radiation

Radiation tends to become an important factor of heat transfer in high temperature applications. The initial wall temperature of the hot head of the Vespel support probe reaches values near *450 K* (Figure 12-7). The surrounding of the probe is close to the ambient temperature, around *293 K*, prior to the test. During the test, the flow around the probe has a temperature around *340 K*. These temperature differences are not sufficient to generate considerable radiative heat fluxes compared to the convective or conductive ones.

More specifically, considering the simple case of a convex surface (such as the ceramic head) exposed to a large isothermal enclosure (such as the surrounding of the ceramic head) is radiating into the enclosure a heat flux given in Eq. (58) (Bejan and Kraus, 2003) that is rewritten for our case in Eq. (59) (Bejan and Kraus, 2003):

$$Q_{RAD} \approx \varepsilon\sigma\left(T^4_{surface} - T^4_{enclosure}\right), \quad (58)$$

$$Q_{RAD} \approx \varepsilon\sigma\left(T^4_{W1} - T^4_{vacuum\ \ or\ air}\right), \quad (59)$$

where ε is the emissivity of the convex surface defined as the ratio of energy emitted by a surface as compared to that of a black surface and $\sigma = 5.670 \times 10^{-8}\ W/m^2/K^4$. Considering the theoretical maximum of the emissivity (for a black body) equal to one, the maximum possible radiative heat flux from the hot head is $1.9\ kW/m^2$ in vacuum and $1.6\ kW/m^2$ during the test. These values are almost one to two orders of magnitude smaller than the calculated wall heat fluxes during the test. Consequently, the influence of the radiation for the temperature differences occurring during the probe operation on the gas temperature calculations is negligible.

15.6 Pulsed heating

Higher spatial resolution on the results of the dual thin film probe can be succeeded by deposing both thin film sensors on the same head (Figure 9-1). Then the wall temperature difference can be generated with a current pulse through one of the two thin film sensors. There are three major difficulties that arise from this new probe design.

First, the two sensors have to be deviated from the stagnation point of the head. Therefore, the heat transfer coefficient *h* should be redefined and a relationship between the calculated gas temperature from Eq. (45) and the real total gas temperature of the flow should be established.

Second, as the pulsed heating is concentrated in a very small area of the probe on the location of one of the two thin film sensors, the lateral conduction effects are of primary importance. Thus, either the heat conduction equation used for the wall heat flux calculations has to be expanded in two dimensions, or the wall heat flux calculated with the existing one dimensional data reduction technique has to be further corrected for the lateral conduction effects.

Third, the pulsed circuit should be designed capable to give sufficient wall temperature difference prior to the test without any possibility of damaging the sensors.

Overcoming the above difficulties and coming up with the new design of the probe require special effort and time and can be a topic of a complete future work.

15.7 References

Bejan A., Kraus A.D., 2003, *'Heat transfer handbook'*, Thermal Radiation, John Wiley & Sons, inc., Hoboken, New Jersey, pp573-633

Miller C.M., 1981, *'Comparison of the thin-film resistance heat-transfer gages with thin-skin transient calorimeter gages in conventional hypersonic wind tunnels'*, NASA Technical Memorandum 83197